Jianying Li ✉
Aokun Wei
Mingyu Yang
Yaqian Wang

https://doi.org/10.21278/TOF.481054623
ISSN 1333-1124
eISSN 1849-1391

RESEARCH ON THE COMPLIANT CONTROL OF ELECTRO-HYDRAULIC SERVO DRIVE FORCE/POSITION SWITCHING FOR A LOWER LIMB EXOSKELETON ROBOT

Summary

In order to improve the flexibility of the foot landing of a lower limb exoskeleton robot based on an electro-hydraulic servo drive and to reduce its impact with the ground, an active compliance control method for force/position switching based on fuzzy control is proposed. According to the mathematical model of each component of the electro-hydraulic servo system of the core drive unit of the lower limb exoskeleton robot, the transfer functions of the position control system and the force control system are obtained respectively, and then its specific working characteristics are studied. Before the feet hit the ground, the position servo control system under the action of a fuzzy controller is used to achieve the movement of legs in free and unconstrained space, and the moment the foot touches the ground, the system is switched to a force servo control system to precisely control the output force, thereby reducing the rigid impact between the feet. In the meantime, the validity of the designed switching method and controller is verified by the joint simulation of MATLAB and AMESIM. The simulation results show that the electro-hydraulic servo force/position switching method based on a fuzzy algorithm is able not only to guarantee the movement accuracy of the foot end of the lower limb exoskeleton robot, but can also effectively reduce the impact force between the foot end and the ground.

Key words: *lower limb exoskeleton robot; electro-hydraulic servo drive; fuzzy algorithm; compliant control; force/position switching*

1. Introduction

With the continuous development of science and technology, especially after the start of the 21st century, Exoskeleton robots as an assistive device for the human body have seen unprecedented growth in the military, civilian, and medical fields [1]. Especially due to China's large population and rapidly aging society, lower extremity rehabilitation exoskeleton robots are increasingly being noticed and intensively investigated by scientists. Research on lower limb rehabilitation robots for patients with limb movement disorders is an important part of rehabilitation robotics research [2-3]. The common drive methods for lower limb exoskeleton robots are those that are motor-driven, pneumatic-driven, and hydraulic-driven. The hydraulic drive method has the advantages of its small size, fast frequency response, and high stability

compared with the other two drive methods and is widely used in lower limb rehabilitation exoskeleton robots [4]. Electro-hydraulic servo lower limb exoskeleton robots achieve complex movements through coordinated movements of the joints of the legs; for free space motion, robot joint drives require high precision position servicing, and the simple and high precision and rigidity of the hydraulic system position servo control, which can meet the control requirements. However, if the electro-hydraulic position servo system is applied directly to the support phase of the robot, there is a high risk of foot-ground shock [5-6]. Lower limb exoskeleton robots are mostly used for patient rehabilitation, but the impact between the foot end and the ground is too great and can cause secondary injuries to patients. Therefore, the exoskeleton robot needs to have a certain degree of suppleness at the moment of switching between the support phase, especially the swing phase and the supporting phase [7]. At present, there is an urgent need for the electro-hydraulic force servo control to improve the flexibility of exoskeleton robot motion, but the force servo response is slow and there are large oscillations and poor tracking accuracy, which cannot be directly applied to the robot's free space motion [8-9].

Scholars have studied many control strategies to address the problem of excessive impact when the foot end of the robot lands on the ground. Koivo and HouShangi used a self-correcting control method to achieve variable gain mixing control to keep the robot end contact force controller parameters at "optimal" values, which has improved the stability of the robot system and the softness of the landing [10]. Fanaei uses a neuro-fuzzy online estimation of an environmental equivalent stiffness contact force compensation method to adapt to robot and environmental parameter changes, which preserves the contact force of the robot and environmental contact control and reduces the impact of robot landing [11]. The DASH Leg designed by Nichol has a torque-controlled hip joint to control the contact force at the moment of touching the ground and a vibration dampening spring at the foot end to achieve active and smooth control of the robot through high precision torque control [12].

Among the research results of domestic scholars, Ren Danmei designed a planar hydraulic biped robot, built an impedance control strategy, and used Adams to build an experimental platform to verify that the equipped impedance control strategy can effectively reduce the impact force on the ground and increase the flexibility of the foot [13]. Bakai first proposed the impedance control method based on force and position, then analysed the influence of different impedance control parameters on the experimental flexibility sensitivity of the hydraulically driven foot robot under different working conditions, and finally obtained the position and force composite impedance control algorithm to achieve the best dynamic flexibility control under dynamic operation [14]. The adaptive impedance control strategy proposed by Ding Qingpeng can identify the environmental stiffness and environmental position, which effectively reduces the steady-state error of foot-end position force tracking. Although it improves the foot suppleness, there is a large response delay [15].

The robot flexibility control methods proposed by the above-mentioned scholars basically use force control or impedance control methods, which can improve the end flexibility of hydraulic robots. However, their structure is complex and the requirements for their dynamic’s models are high, so they are not particularly suitable for the flexibility control of electro-hydraulic servo-driven rehabilitation lower limb exoskeleton robots at the moment of the foot touching the ground. Therefore, in order to effectively reduce the impact of the lower limb exoskeleton robot at the moment of landing on the foot end, so that the foot end is in gentle contact with the ground, this paper combines the advantages of a force servo system and a position servo system, and proposes an active soft control method for force/position switching based on fuzzy control, so that the smooth switching of the desired position control and the desired contact force control of the foot end of the lower limb exoskeleton robot is achieved. This provides an effective way to solve the foot-ground impact generated by the foot end of the exoskeleton robot at the moment of landing.

2. Modelling of an electro-hydraulic servo drive system for a lower limb exoskeleton robot

Each single leg of the lower limb exoskeleton robot is composed of electro-hydraulic servo actuators and shock absorbing springs as its power drive system and shock absorbing links and is solidly connected to them through the back frame and the rods that simulate the thigh bone and the lower leg bone. Its composition assembly schematic is shown in Figure 1.

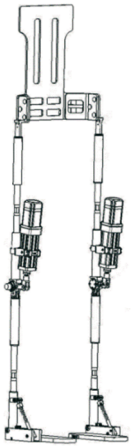

Fig. 1 Schematic diagram of the overall assembly of the lower limb exoskeleton robot

Since this paper focuses on the flexibility of the lower limb exoskeleton robot based on an electro-hydraulic servo drive before and after the moment of landing on one leg, the control characteristics at the knee joint of one leg are mainly considered, and its structural sketch is shown in Figure 2. In the Figure, a, b and c are the thigh, calf, and foot of the exoskeleton robot, τ_1, τ_2 and τ_3 are the rotational moments of each joint of the exoskeleton robot respectively, h is the height of the foot end of the lower limb of the exoskeleton robot off the ground, and d is the hydraulic drive system of the leg.

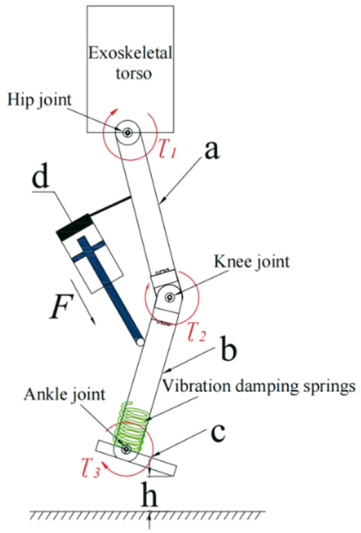

Fig. 2 Sketch of the single-leg structure of the hydraulic exoskeleton robot

The high-precision flexible control performance of the single-leg knee electro-hydraulic servo drive system is directly related to the motion control performance of the whole robot in the walking process, so the knee electro-hydraulic servo drive unit is a high-power density integrated valve-controlled cylinder structure. Its assembly schematic is shown in Figure 3 [16].

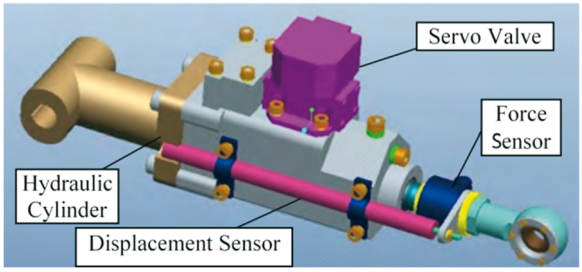

Fig. 3 Schematic diagram of the electro-hydraulic servo drive unit assembly for the single leg knee joint

2.1 Kinematics and dynamics analysis of the lower limb exoskeleton robot

In the process of the lower limb exoskeleton robot assisting the wearer's movement, the human lower limb and the mechanical lower limb of the lower limb exoskeleton robot are taken as a whole, and the kinematic model is established as shown in Figure 4. The D-H coordinate system is established by the D-H method to obtain the D-H parameter table as shown in Table 1.

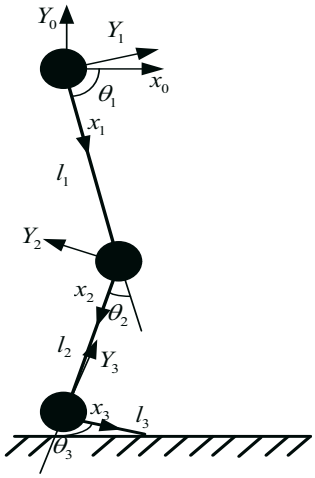

Fig. 4 Kinematic model of the hydraulic lower limb exoskeleton robot

Table 1 The D-H parameters

Joint i	$\theta_i(°)$	$d_i(m)$	$a_i(m)$	$\alpha_i(°)$
1	θ_1	0	l_1	0
2	θ_2	0	l_2	0
3	θ_3	0	l_3	0

Since the motion of each joint of the lower limb is in the form of rotation, the D-H method is chosen to define the rules for each joint rod as:

(1) The rod angle a_i is the angle turned around the x_i axis from the z_i axis to the axis z_{i+1};

(2) The rod length a_i is the distance between axis i and axis i+1;

(3) The rod offset d_i is the distance along the z_i axis from the x_{i-1} axis to the x_i axis;

(4) The rod rotation angle θ_i is the angle turned around the z_i axis from the x_{i-1} axis to the x_i axis.

By solving the matrix for each joint of the lower limb through the parameters in the table, the corresponding postural relationship is obtained:

$$\begin{aligned} {}^{i-1}A_i &= R(x_i,\alpha_i)\,\mathrm{Trans}(x_i,\alpha_i)\,\mathrm{Trans}(z_i,d_i)R(z_i,\theta_i) \\ &= \begin{bmatrix} c\theta_i & -s\theta_i c\alpha_i & 0 & a_i c\theta_i \\ s\theta_i & c\theta_i c a_i & -s a_i & a_i s\theta_i \\ 0 & s a_i & c a_i & d_i \\ 0 & 0 & 0 & 1 \end{bmatrix} \end{aligned} \tag{1}$$

In this case, to simplify the matrix expression, s denotes sin and c denotes cos. Thus, the flush coordinate transformation matrix between each joint linkage is: ${}^{0}_{N}T = {}^{0}_{1}T\,{}^{1}_{2}T\,{}^{2}_{3}T\cdots{}^{N-1}_{N}T$.

The final expression of the joint matrix obtained is:

$${}^{0}_{3}T = {}^{0}_{1}T\,{}^{1}_{2}T\,{}^{2}_{3}T = \begin{bmatrix} n_x & o_x & 0 & p_x \\ n_y & o_y & 0 & p_y \\ 0 & 0 & 1 & 0 \\ 0 & 0 & 0 & 1 \end{bmatrix}. \tag{2}$$

Among them:

$$\begin{cases} n_x = c(\theta_1+\theta_2+\theta_3) \\ n_y = s(\theta_1+\theta_2+\theta_3) \\ o_x = -s(\theta_1+\theta_2+\theta_3) \\ o_y = c(\theta_1+\theta_2+\theta_3) \\ p_x = l_1 c\theta_1 + l_2 c(\theta_1+\theta_2) + l_3 c(\theta_1+\theta_2+\theta_3) \\ p_y = l_1 s\theta_1 + l_2 s(\theta_1+\theta_2) + l_3 s(\theta_1+\theta_2+\theta_3) \end{cases}. \tag{3}$$

The inverse kinematic analysis is then performed to calculate the angle of rotation required for each joint, which is solved by the joint cubic equation, according to the formula ${}^{0}T_3 = {}^{0}T_1 \cdot {}^{1}T_2 \cdot {}^{2}T_3$, and we get ${}^{0}T_1^{-1} \cdot {}^{0}T_3 = {}^{1}T_2 \cdot {}^{2}T_3$, and then we perform variable substitution ${}^{0}T_1^{-1} \cdot {}^{0}T_3 = T1$, ${}^{1}T_2 \cdot {}^{2}T_3 = T2$ and $T1 = T2$ obtains the rotation angle of each joint.

Angle of rotation of the hip joint:

$$\theta_1 = \arcsin\left(\frac{x^2+y^2-l_1^2-l_2^2}{2l_2\sqrt{x^2+y^2}}\right) - \arctan\frac{x}{y} \tag{4}$$

Knee joint rotation angle:

$$\theta_2 = \arccos\left(\frac{x^2+y^2-l_1^2-l_2^2}{2l_1 l_2}\right) \tag{5}$$

Angle of rotation of the ankle joint:

$$\begin{aligned} \theta_3 = \theta &- \arcsin\left(\frac{x^2+y^2-l_1^2-l_2^2}{2l_2\sqrt{x^2+y^2}}\right) + \arctan\frac{x}{y} \\ &- \arccos\left(\frac{x^2+y^2-l_1^2-l_2^2}{2l_1 l_2}\right) \end{aligned}. \tag{6}$$

The dynamics modelling analysis of the hydraulic lower limb exoskeleton robot using the Lagrange method is shown in Figure 5.

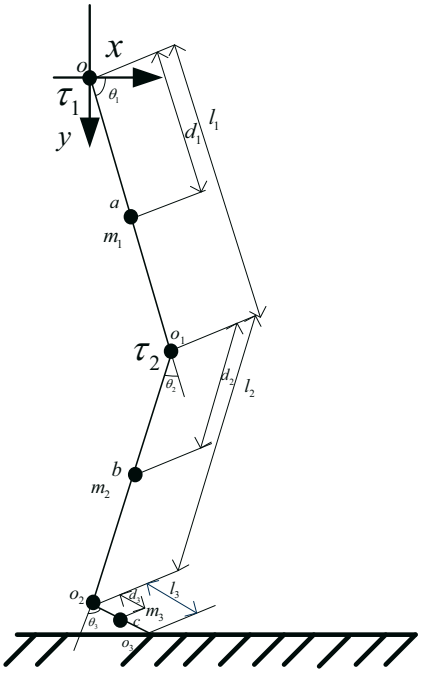

Fig. 5 Dynamics model of the hydraulic lower limb exoskeleton robot

In the Figure, τ_1 and τ_2 are the torque of the hip and knee joints of the lower limb drive joints, m_1, m_2 and m_3 are the weights of the thigh structure, calf structure, and ankle joint of the lower limb and the foot, l_1 and l_2 are the design lengths of the thigh and calf structures, θ_1, θ_2 and θ_3 are the angles of action of each joint of the lower limb, and d_1, d_2 and d_3 are the straight line lengths from the centre of mass of the thigh and calf and foot to their connecting joints. I_1, I_2 and I_3 are the rotational inertia of the thigh structure, the calf structure, and the foot.

From the analysis it can be concluded that:

The equations of the lower limb structure thigh E_{k1} with E_{p1} are shown as:

$$E_{k1} = \frac{1}{2} I_1 \dot{w_1}^2 = \frac{1}{2} m_1 d_1^2 \dot{\theta_1}^2 \tag{7}$$

$$E_{p1} = m_1 g d_1 \sin\theta_1 \tag{8}$$

The velocities v_b and v_c of the centre of mass of the calf rod and foot can be obtained by differentiation according to the coordinate positions.

By simplification, we get:

$$v_b^2 = \dot{x_5}^2 + \dot{y_5}^2 \tag{9}$$

$$v_c^2 = \dot{x_6}^2 + \dot{y_6}^2 \tag{10}$$

By simplification, we get:

$$v_b^2 = l_1^2 \dot{\theta_1}^2 + 2 l_1 d_2 \cos\theta_2 \dot{\theta_1}(\dot{\theta_1} + \dot{\theta_2}) + d_2^2(\dot{\theta_1} + \dot{\theta_2})^2 \tag{11}$$

The lower limb structure calf E_{k2} with E_{p2} is expressed as:

$$\begin{aligned} E_{k2} &= \frac{1}{2} I_2 w_2^{\ 2} + \frac{1}{2} m_2 v_b^{\ 2} \\ &= \frac{1}{2} m_2 d_2^{\ 2} \dot{\theta}_2^{\ 2} + \frac{1}{2} m_2 l_1^{\ 2} \dot{\theta}_1^{\ 2} + m_2 l_1 d_2 \cos\theta_2 \dot{\theta}_1 (\dot{\theta}_1 + \dot{\theta}_2) + \frac{1}{2} m_2 d_2^{\ 2} (\dot{\theta}_1 + \dot{\theta}_2)^2 \end{aligned} \tag{12}$$

$$E_{p2} = m_2 g (l_1 \sin\theta_1 + d_2 \sin(\theta_1 + \theta_2)) \tag{13}$$

The expressions for the legs E_{k3} and E_{p3} are

$$E_{k3} = \frac{1}{2} I_3 w_3^{\ 2} + \frac{1}{2} m_3 v_c^{\ 2} \tag{14}$$

$$E_{p3} = m_3 g (l_1 \sin\theta_1 + l_2 \sin(\theta_1 + \theta_2) + d_3 \sin(\theta_1 + \theta_2 - \theta_3)) \tag{15}$$

To facilitate the analysis of the lower limb structures, it was determined that the masses of the lower leg, ankle, and foot were concentrated at the ankle structure of the lower limb and marked as m_3.

According to the above obtained $v_{o2}^{\ 2}$:

$$v_o^{\ 2} = l_1^{\ 2} \dot{\theta}_1^{\ 2} + 2 l_1 l_2 \cos\theta_2 \dot{\theta}_1 (\dot{\theta}_1 + \dot{\theta}_2) + l_2^{\ 2} (\dot{\theta}_1 + \dot{\theta}_2)^2 \tag{16}$$

The resulting expression after correction is:

$$\begin{aligned} E_{k2}^{\ *} &= \frac{1}{2} I_2 w_2^{\ 2} + \frac{1}{2} m_2 v_b^{\ 2} + \frac{1}{2} m_3 v_{o2}^{\ 2} \\ &= \frac{1}{2} m_2 d_2^{\ 2} \dot{\theta}_2^{\ 2} + \frac{1}{2} m_2 l_1^{\ 2} \dot{\theta}_1^{\ 2} + m_2 l_1 d_2 \cos\theta_2 \dot{\theta}_1 (\dot{\theta}_1 + \dot{\theta}_2) + \frac{1}{2} m_2 d_2^{\ 2} (\dot{\theta}_1 + \dot{\theta}_2)^2 \\ &+ \frac{1}{2} m_3 l_1^{\ 2} \dot{\theta}_1^{\ 2} + m_3 l_1 l_2 \cos\theta_2 \dot{\theta}_1 (\dot{\theta}_1 + \dot{\theta}_2) + \frac{1}{2} m_3 l_2^{\ 2} (\dot{\theta}_1 + \dot{\theta}_2)^2 \\ &= \frac{1}{2} m_2 d_2^{\ 2} \dot{\theta}_2^{\ 2} + \frac{1}{2} l_1^{\ 2} \dot{\theta}_1^{\ 2} (m_2 + m_3) + \\ &\quad l_1 \cos\theta_2 \dot{\theta}_1 (\dot{\theta}_1 + \dot{\theta}_2)(m_2 d_2 + m_3 l_2) + \frac{1}{2} (\dot{\theta}_1 + \dot{\theta}_2)^2 (m_2 d_2^{\ 2} + m_3 l_2^{\ 2}) \end{aligned} \tag{17}$$

The single-leg structural model can be treated as a two-link mechanism when performing analytical calculations. Its corresponding Lagrangian function *L* is:

$$\begin{aligned} E_{p2}^{\ *} &= m_2 g (l_1 \sin\theta_1 + d_2 \sin(\theta_1 + \theta_2)) + m_3 g (l_1 \sin\theta_1 + l_2 \sin(\theta_1 + \theta_2)) \\ &= g l_1 \sin\theta_1 (m_2 + m_3) + g \sin(\theta_1 + \theta_2)(m_2 d_2 + m_3 l_2) \end{aligned} \tag{18}$$

$$L = E_{k1} + E_{k2}^{\ *} - E_{p1} - E_{p2}^{\ *} \tag{19}$$

The derivative for the Lagrangian function L:

$$\frac{\partial L}{\partial \dot{\theta}_1} = m_1 d_1^{\,2}\,\dot{\theta}_1 + l_1^{\,2}\,\dot{\theta}_1 (m_2 + m_3) + l_1 \cos\theta_2 (m_2 d_2 + m_3 l_2)(2\dot{\theta}_1 + \dot{\theta}_2) + (m_2 d_2^{\,2} + m_3 l_2^{\,2})(\dot{\theta}_1 + \dot{\theta}_2) \tag{20}$$

$$\frac{\mathrm{d}}{\mathrm{d}t}\left(\frac{\partial L}{\partial \dot{\theta}_1}\right) = m_1 d_1^{\,2}\,\ddot{\theta}_1 + l_1^{\,2}\,\ddot{\theta}_1 (m_2 + m_3) + l_1 \cos\theta_2 (m_2 d_2 + m_3 l_2)(2\ddot{\theta}_1 + \ddot{\theta}_2) - (2\dot{\theta}_1 + \dot{\theta}_2)\dot{\theta}_2\, l_1 \sin\theta_2 (m_2 d_2 + m_3 l_2) + (m_2 d_2^{\,2} + m_3 l_2^{\,2})(\ddot{\theta}_1 + \ddot{\theta}_2) \tag{21}$$

$$\frac{\partial L}{\partial \theta_1} = -m_1 g d_1 \cos\theta_1 - g l_1 \cos\theta_1 (m_2 + m_3) - g\cos\left(\theta_1 + \theta_2\right)(m_2 d_2 + m_3 l_2) \tag{22}$$

$$\frac{\partial L}{\partial \dot{\theta}_2} = m_2 d_2^{\,2}\,\dot{\theta}_2 + l_1 \cos\theta_2\,\dot{\theta}_1 (m_2 d_2 + m_3 l_2) + (m_2 d_2^{\,2} + m_3 l_2^{\,2})(\dot{\theta}_1 + \dot{\theta}_2) \tag{23}$$

$$\frac{\mathrm{d}}{\mathrm{d}t}\left(\frac{\partial L}{\partial \dot{\theta}_2}\right) = m_2 d_2^{\,2}\,\ddot{\theta}_2 + l_1 \cos\theta_2\,\ddot{\theta}_1 (m_2 d_2 + m_3 l_2) - l_1\,\dot{\theta}_2 \sin\theta_2\,\dot{\theta}_1 (m_2 d_2 + m_3 l_2) + (m_2 d_2^{\,2} + m_3 l_2^{\,2})(\ddot{\theta}_1 + \ddot{\theta}_2) \tag{24}$$

$$\frac{\partial L}{\partial \theta_2} = -l_1 \sin\theta_2\,\dot{\theta}_1 (\dot{\theta}_1 + \dot{\theta}_2)(m_2 d_2 + m_3 l_2) - g\cos\left(\theta_1 + \theta_2\right)(m_2 d_2 + m_3 l_2) \tag{25}$$

Thus, the moment equations for the hip joint τ_1 and knee joint τ_2 can be obtained by the equation below:

$$\begin{aligned}\tau_1 &= \frac{\mathrm{d}}{\mathrm{d}t}\left(\frac{\partial L}{\partial \dot{\theta}_1}\right) - \frac{\partial L}{\partial \theta_1} \\ &= m_1 d_1^{\,2}\,\ddot{\theta}_1 + l_1^{\,2}\,\ddot{\theta}_1 (m_2 + m_3) + l_1 \cos\theta_2 (m_2 d_2 + m_3 l_2)(2\ddot{\theta}_1 + \ddot{\theta}_2) \\ &\quad - (2\dot{\theta}_1 + \dot{\theta}_2)\dot{\theta}_2\, l_1 \sin\theta_2 (m_2 d_2 + m_3 l_2) + (m_2 d_2^{\,2} + m_3 l_2^{\,2})(\ddot{\theta}_1 + \ddot{\theta}_2) \\ &\quad + m_1 g d_1 \cos\theta_1 + g l_1 \cos\theta_1 (m_2 + m_3) + g\cos\left(\theta_1 + \theta_2\right)(m_2 d_2 + m_3 l_2)\end{aligned} \tag{26}$$

$$\begin{aligned}\tau_2 &= \frac{\mathrm{d}}{\mathrm{d}t}\left(\frac{\partial L}{\partial \dot{\theta}_2}\right) - \frac{\partial L}{\partial \theta_2} \\ &= m_2 d_2^{\,2}\,\ddot{\theta}_2 + l_1 \cos\theta_2\,\ddot{\theta}_1 (m_2 d_2 + m_3 l_2) - l_1\,\dot{\theta}_2 \sin\theta_2\,\dot{\theta}_1 (m_2 d_2 + m_3 l_2) \\ &\quad + (m_2 d_2^{\,2} + m_3 l_2^{\,2})(\ddot{\theta}_1 + \ddot{\theta}_2) + l_1 \sin\theta_2\,\dot{\theta}_1 (\dot{\theta}_1 + \dot{\theta}_2)(m_2 d_2 + m_3 l_2) \\ &\quad + g\cos\left(\theta_1 + \theta_2\right)(m_2 d_2 + m_3 l_2)\end{aligned} \tag{27}$$

The kinematic relationships of the exoskeleton lower limb, including the joint angles, the end effector positions, etc., are described by mathematical models. The electro-hydraulic servo actuator controls the joint angle of the exoskeleton lower limb and provides information such

as the corresponding displacement and velocity feedback [17]. A mathematical model is used to describe the dynamics of the exoskeleton lower limb, including mass, inertia, torque, and control inputs. The electro-hydraulic servo actuator assists the movement of the exoskeleton lower limb by providing a certain torque or force and controls it according to the dynamics of the exoskeleton.

2.2 Mathematical model of the electro-hydraulic servo drive unit position control

(1) Let us assume that the bulk modulus of elasticity and temperature of the fluid are kept constant, the pressure in the closed cavity of the hydraulic actuator is equal everywhere, and the leakage is laminar flow. Considering the worst case of system stability, the basic equation of the valve-controlled cylinder system is obtained with the piston rod in the neutral position as the reference [18].

$$\begin{cases} Q_L = K_q X_v - K_c P_L \\ Q_L = A_1 s X_P + C_{tp} P_L + C_{tc} P_s + \dfrac{V_t}{4\beta_e} s P_L \\ A_1 P_L = m_t s^2 X_P + B_p s X_P + K X_P + F_L \end{cases}, \tag{28}$$

where K_q is the flow gain coefficient, X_{v} is the displacement of the spool/m, K_c is the flow and pressure coefficient, P_L is the system output pressure/MPa, Q_L is the load flow/m^3/s, A_{p} is the effective area of the actuator/m^2, X_p is the maximum stroke of the cylinder/m, C_{tp} is the combined leakage coefficient of the actuator/$\mathrm{m}^5/\mathrm{N}\cdot\mathrm{m}$, β_e is the effective volume modulus of elasticity/$\mathrm{N}\cdot\mathrm{m/s}$, V_t is the equivalent volume of the oil chamber/m^3, K is the equivalent spring stiffness of the hydraulic cylinder/N/m, m_t for load quality, and B_p is the damping factor.

The transfer function model of the displacement of the foot end after combining the above three equations is shown in Equation (2):

$$X_p = \frac{\dfrac{K_q}{A_p} X_v - \dfrac{K_{ce}}{A_p^2}\left(1 + \dfrac{V_t}{4\beta_e K_{ce}} s\right) F_L}{\dfrac{m_t V_t}{4\beta_e A_p^2} s^3 + \left(\dfrac{m_t K_{ce}}{A_p^2} + \dfrac{V_t}{4\beta_e A_p^2}\right) s^2 + \left(1 + \dfrac{B_p K_{ce}}{A_p^2} + \dfrac{K V_t}{4\beta_e A_p^2}\right) s + \dfrac{K K_{ce}}{A_p^2}} \tag{29}$$

$$K_{ce} = K_c + C_{tp}, \tag{30}$$

where K_{ce} is the total flow rate - Pressure coefficient.

Since the viscous damping factor β_e is generally small again, the velocity of the piston resulting from the leakage flow caused by viscous friction is much smaller than the velocity of the movement of the piston, that is [19]

$$\frac{B_p K_{ce}}{A_p^2} \ll 1. \tag{31}$$

Therefore, the system equation can be simplified as

$$G_L(\mathrm{s}) = \frac{X_p}{X_v} = \frac{\dfrac{1}{A_p}}{s\left[\dfrac{s^2}{w_h^2} + \dfrac{2\xi_h}{w_h}s + 1\right]}, \tag{32}$$

where w_h is the natural frequency of the hydraulic pressure /rad/s and ξ_h is the damping ratio of the hydraulic pressure.

Among them, $w_h = \sqrt{\dfrac{4\beta_e A_p^2}{V_t m_t}}$ $\xi_h = \dfrac{K_{ce}}{A_p}\sqrt{\dfrac{\beta_e m_t}{V_t}} + \dfrac{B_p}{4A_p}\sqrt{\dfrac{V_t}{\beta_e m_t}}$.

(2) The servo amplifier output current Δi is approximately proportional to the output voltage u_g. The transfer function can be expressed by the servo amplifier K_a, that is [20]

$$\frac{I(s)}{U(s)} = K_a, \tag{33}$$

where I is the output current of the amplifier, K_a is the servo amplifier gain, and U is the input voltage signal /V.

(3) When the inherent bandwidth of the servo valve is much higher than the inherent frequency of the power element, the transfer function of the servo valve can be regarded as a proportional unit:

$$G_v(\mathrm{s}) = \frac{X(\mathrm{s})}{I(\mathrm{s})} = K_v, \tag{34}$$

where $G_v(\mathrm{s})$ is the electro-hydraulic servo valve transfer function, and K_v is the electro-hydraulic servo valve flow gain.

Therefore, the transfer function of the electro-hydraulic servo valve is

$$G_u(\mathrm{s}) = \frac{X(\mathrm{s})}{U(\mathrm{s})} = K_v K_a = K_u. \tag{35}$$

(4) The displacement sensor is often used in an electro-hydraulic position servo system, and its transfer function can be considered as a proportional loop section [21], that is:

$$U_f = K_m x_p, \tag{36}$$

where U_f is the displacement feedback signal, and K_m is the displacement sensor coefficient.

Based on the above equations, a system block diagram for position control can be drawn, as shown in Figure 6.

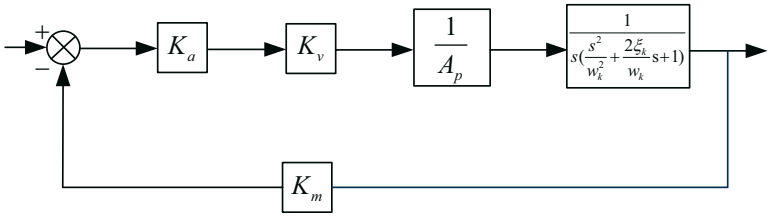

Fig. 6 Position control

The resulting open-loop transfer function of the electro-hydraulic servo position system is:

$$G(s)=\frac{\frac{K_a K_v K_m}{A_p}}{s\left[\frac{s^2}{w_h^2}+\frac{2\xi_h}{w_h^2}s+1\right]}. \tag{37}$$

2.3 Mathematical model of the hydraulic drive unit force control

Treating the transfer function of the force transducer as a proportional link, we get [22]

$$U_{fF}=K_{fF}F_p, \tag{38}$$

where K_{fF} is the force sensor coefficient (V/N) and F_p is the hydraulic cylinder output force (N).

Regardless of the position control system or force control system, the mechanism modelling is based on the hydraulic drive unit structure, so the basic equations of the valve-controlled cylinder system and the servo valve equation are the same. Therefore, according to the above equations, a sketch of the force control system can be drawn as shown in Figure 7:

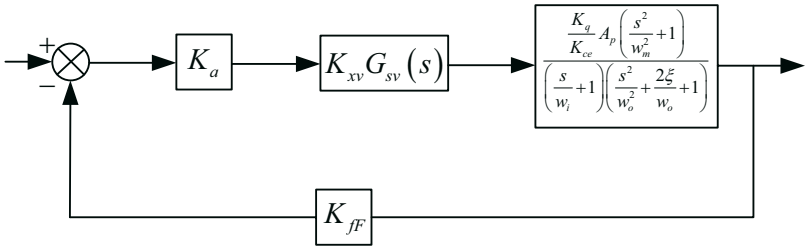

Fig. 7 Force control system

The transfer function of the spool displacement X_v to the hydraulic cylinder output force F_g can be obtained from the block diagram:

$$\frac{F_g}{X_v}=\frac{\frac{K_q}{A_p}K\left(\frac{m_t}{K}s^2+\frac{B_p}{K}s+1\right)}{\frac{V_t m_t}{4\beta_e A_p^2}s^3+\left(\frac{K_{ce}m_t}{A_p^2}+\frac{V_t B_p}{4\beta_e A_p^2}\right)s^2+\left(1+\frac{K_{ce}B_p}{A_p^2}+\frac{V_t K}{4\beta_e A_p^2}\right)s+\frac{K_{ce}K}{A_p^2}}, \tag{39}$$

where k is the load spring stiffness and $\frac{4\beta_e A_p^2}{V_t}$ is the hydraulic spring stiffness. Usually, the load damping B_p is very small and can be neglected.

If the condition $\left[\frac{K_{ce}\sqrt{Km_t}}{A_p^2\left(1+V_tK/4\beta_e A_p^2\right)}\right]\ll 1$ is met, then simplify to get

$$\frac{F_g}{X_v}=\frac{\frac{K_q}{A_p}A_p\left(\frac{s^2}{w_m^2}+1\right)}{\left(\frac{s}{w_r}+1\right)\left(1+\frac{s^2}{w_0^2}+\frac{2\zeta_0}{w_0}\right)}, \tag{40}$$

where w_m is the inherent frequency of the load, $w_m=\sqrt{K/m_t}$, w_r is the ratio of the stiffness to the damping factor of the hydraulic spring coupled in series with the load spring,

$w_r = \frac{K_{ce}}{A_p^2} \Big/ \left(\frac{V_t}{4\beta_e A_p^2} + \frac{1}{k} \right)$, w_0 is the inherent frequency of the load mass travel of the hydraulic spring coupled in parallel with the load spring, and $w_0 = w_m \sqrt{1 + \frac{4\beta_e A_p^2}{KV_t}}$, ζ_0 is the damping ratio, $\zeta_0 = \frac{1}{2w_o} \frac{1}{V_t \left[1 + \left(KV_t / 4\beta_e A_p^2 \right) \right]}$.

Therefore, the open-loop transfer function of the system is

$$G_{(s)}H_s = \frac{G_{fv}K_o \left(\frac{s^2}{w_m^2} + 1 \right)}{\left(\frac{s}{w_r} + 1 \right) \left(\frac{s^2}{w_o^2} + \frac{1}{w_o} + 1 \right)}, \tag{41}$$

where K_o is the open-loop gain of the system $K_0 = K_a K_{sv} A_p K_{fF} K_q / K_{ce}$.

3. Switching control of the foot end position and force for the lower limb exoskeleton robot

3.1 Principle of position and force switching control

Physical contact control between the robot and the environment is the basis of the robot application of limb rehabilitation training tasks. Exoskeleton robots will generate large contact forces with the ground in the process of landing, and therefore the traditional robot control system based only on position control can no longer meet the requirements of contact between the robot and the environment [23]. When the electro-hydraulic servo exoskeleton robot is in contact with the ground, the ground constrains the motion of the electro-hydraulic servo system in order to meet the accuracy of the foot-end movement and at the same time to avoid large foot-end impact when the exoskeleton robot is in contact with the ground. The use of force/position switching control is an effective control method.

Both position control and force control servo systems use fuzzy PID controllers. Before the exoskeleton robot's foot contacts the ground, the position control servo system works and achieves foot-end motion accuracy. However, the moment the exoskeleton robot's foot contacts the ground, the system will experience a large shock, and then the force control servo system works to reduce the generation of parameter jumps and jitter. In this paper, the electro-hydraulic servo force/position switching method based on a fuzzy algorithm is able not only to realize the accuracy of the foot-end movement of the exoskeleton robot but also to effectively reduce the impact force between the foot-end and the ground. The control schematic is shown in Figure 8:

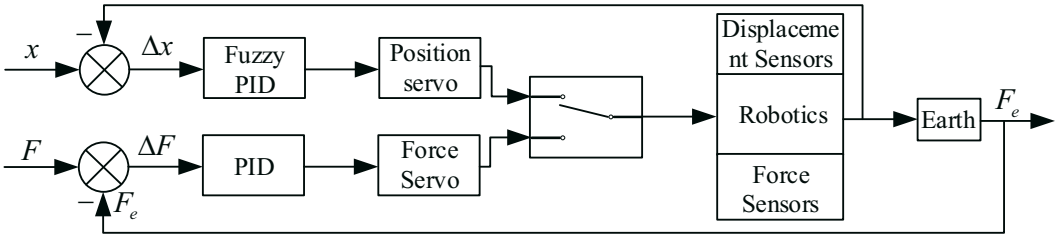

Fig. 8 Electro-hydraulic servo lower limb exoskeleton machine manpower switching schematic

3.2 Design of the controller

(1) Principle of the fuzzy PID controller

Fuzzy control is based on fuzzy mathematics, combined with the control rules summarised by expert experience, and uses the principle of fuzzy reasoning to fuse and derive multi-source data, so that the controlled object can be effectively controlled [24]. Compared with conventional control methods, fuzzy control does not rely on accurate mathematical models and is more robust to external disturbances and system parameters. The fuzzy PID controller adjusts the PID control parameters online based on fuzzy inference, giving the system high stability and responsiveness in the face of uncertainty and nonlinearity [25]. Its structure block diagram is shown in Figure 9.

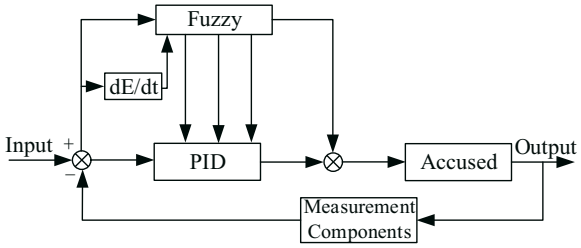

Fig. 9 Block diagram of fuzzy PID controller structure

Fuzzy control includes fuzzy processing, fuzzy control operation, and fuzzy judgment. The two input parameters are the systematic error E and the error variable rate EC, the output is the correction parameter of the PID controller as *dkp* , *dki* ,and *dkd* , the domain of the variables' input according to the fuzzy partition theory is $\{-1,-0.8,-0.6,-0.4,-0.2,0,0.2,0.4,0.6,0.8,1\}$, and the systematic error of the input variables and the error rate theoretical domain are $\{-1,-0.8,-0.6,-0.4,-0.2,0,0.2,0.4,0.6,0.8,1\}$. The affiliation function is a quantitative description of a fuzzy concept, commonly used in Gaussian illusions, trigonometric functions, S-shaped functions, etc. The Gaussian affiliation function has the characteristics of a simple structure, a small computational workload, and high accuracy, and therefore the affiliation curve of this control variable is described by a Gaussian affiliation function. The affiliation function curves of the input variables are shown in Figure 10, and the affiliation function curves of the output variables are shown in Figure 11:

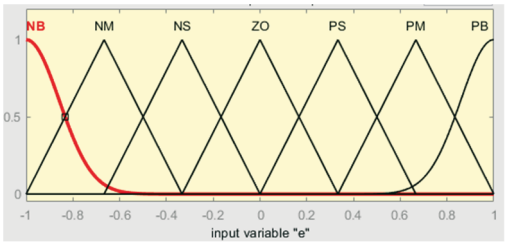

Fig. 10 Input variable e affiliation function curve

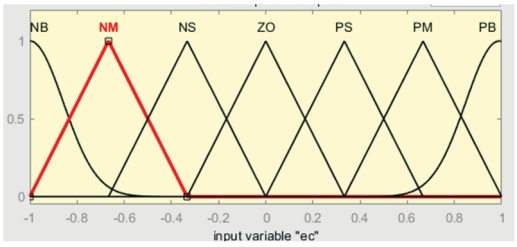

Fig. 11 Output variable ec affiliation function curve

(2) Create a fuzzy rule table

Fuzzy rule design plays a key role in the effect of fuzzy control. According to the adjustment rules of control parameters, combined with the valuable experience of experts in the actual control process, the control rules for the three parameters *dkp*, *dki* and *dkd* can be designed as shown in Table 2, Table 3, and Table 4:

Table 2 *dkp* of fuzzy rule table

e \ ec	NB	NM	NS	ZO	PS	PM	PB
NB	PB	PB	PB	PB	PS	ZO	NS
NM	PB	PB	PM	PM	ZO	NS	NM
NS	PB	PM	PM	PS	NS	NM	NB
ZO	ZO	ZO	ZO	ZO	ZO	ZO	ZO
PS	NB	NM	NS	PS	PM	PM	PB
PM	NM	NS	ZO	PM	PB	PB	PB
PB	NS	ZO	PS	PB	PB	PB	PB

Table 3 *dki* of fuzzy rule table

e \ e_c	NB	NM	NS	ZO	PS	PM	PB
NB	PB	PB	PB	PB	NS	NM	NB
NM	PB	PB	PM	PM	NM	NB	NB
NS	PB	PM	PS	PS	NB	NB	NB
ZO	ZO	ZO	ZO	ZO	ZO	ZO	ZO
PS	NB	NB	NB	PS	PS	PM	PB
PM	NB	NB	NM	PM	PM	PB	PB
PB	NB	NM	NS	PB	PB	PB	PB

Table 4 *dkd* of fuzzy rule table

e \ e_c	NB	NM	NS	ZO	PS	PM	PB
NB	PB	PB	PB	NB	NM	NM	NS
NM	PB	PB	PM	NM	ZO	PS	PM
NS	PB	PM	PM	NS	PM	PB	PB
ZO	ZO	ZO	ZO	ZO	ZO	ZO	ZO
PS	PB	PB	PM	NS	PM	PM	PB
PM	PM	PS	ZO	NM	PM	PB	PB
PB	NS	NM	NB	NB	PB	PB	PB

Each subset in the table represents a fuzzy rule, so 49 fuzzy rules need to be written in the Fis file, as shown in Figure 12.

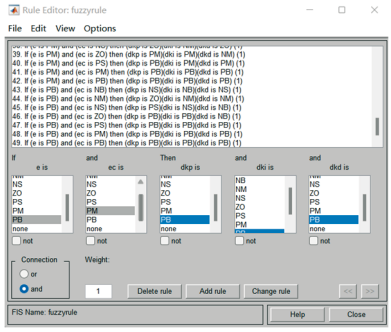

Fig. 12 Fis rule diagram

(3) Obtain the fuzzy rule surface map

Use MATLAB to view the fuzzy rule surface plots of A, B, and C, as shown in Figure 13.

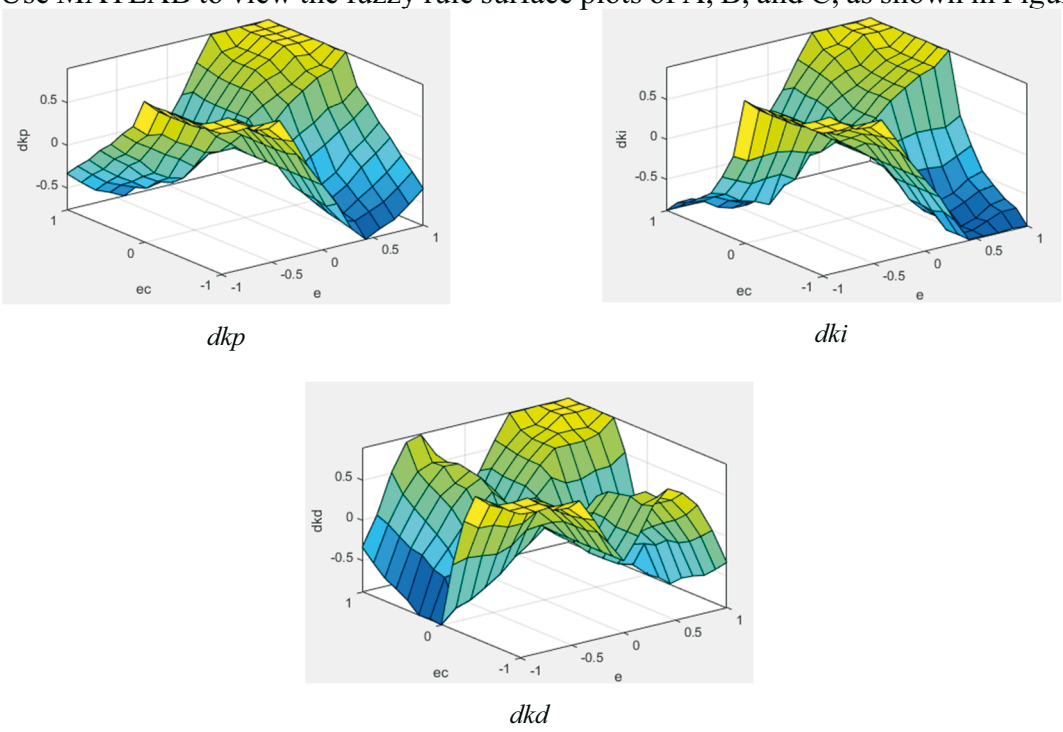

dkp *dki*

dkd

Fig. 13 Fuzzy rule surface diagram

The fuzzy controller fuzzifies the difference between input and output e and the rate of change of the difference ec, starts reasoning based on the rule table, calculates the affiliation values of the three PID parameters, and finally defuzzifies and outputs the corrected ΔK_P, ΔK_I, and ΔK_D parameter values to achieve real-time dynamic adjustment of the PID control parameters and improve the system response characteristics. The final parameters of the fuzzy PID controller are obtained as:

$$\begin{cases} K_P = K_{P0} + \Delta K_P \\ K_I = K_{I0} + \Delta K_I \\ K_D = K_{D0} + \Delta K_D \end{cases}, \tag{42}$$

where K_{P0}, K_{I0}, and K_{D0} are the original values of the PID controller parameters.

4. AMEsim and Matlab joint simulation

AMEsim is advanced modelling and simulation software that presents the concept of basic elements so that no program code needs to be written, and the functions of systems and components can be described simply by extracting the smallest units from the system model. It can also be combined with many other types of software, such as Matlab, Adams, Labview, etc [26]. The lower limb exoskeleton robot servo system is more complex, containing a variety of hydraulic components and mechanical motion mechanism. Simulation using Simulink or AMESim software alone requires great computational work and may not yield more accurate simulation results. Therefore, Simulink is combined with AMESim software for joint simulation, applying the powerful tool library in the AMESim software. The components in the library were set with some of the key parameters, eliminating a large amount of calculation work. By using Simulink software to build the control system and borrowing its powerful data analysis and calculation capability to simulate the hydraulic drive system model built in

AMESim software, the lower limb exoskeleton robot servo system can be analysed as a whole, making the simulation results more representative and accurate [27].

The model of the exoskeleton robot human position switching servo system is built according to AMEsim software as shown in Figure 14, the model parameters of each unit are set by the author. The parameters are shown in Tables 5, 6 and 7. The Simulink module of Matlab is run to get the S function of the system. It is not necessary to calculate the mathematical model of the system to obtain the transfer function.

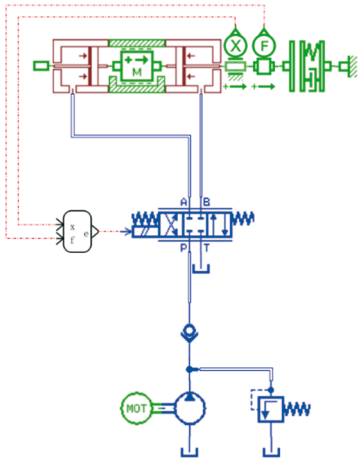

Fig. 14 Amesim model of the electro-hydraulic force level switching servo system for the exoskeleton robot

Table 5 Motor technical parameters

Model	Power rating	Rated current	Rated speed
Y132S-6	3 kW	3 A	960 r/min

Table 6 Servo valve technical parameters

Components	Model	Rated flow rate	Rated pressure
Hydraulic valve	FF102/30	10 L/min	21 MPa
Relief valve	YF-L8H4	20 L/min	31.5 MPa

Table 7 Hydraulic pump technical parameters

Model	Displacement	Maximum pressure	Rated speed	Maximum speed	Drive power
AP100/5D818	5 cm^3/rev	21 MPa	1800 r/min	3500 r/min	2.2 kW

The simulation time is set to 14 s and the number of simulation steps is 500. The simulation process is shown in Figure 15 and the simulation results are shown in Figure 16.

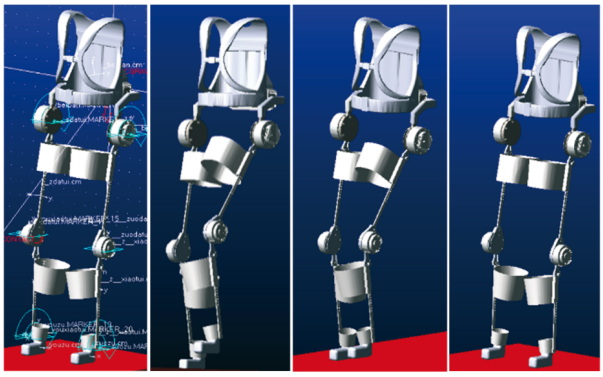

Fig. 15 Adams simulation process of the lower limb exoskeleton robot

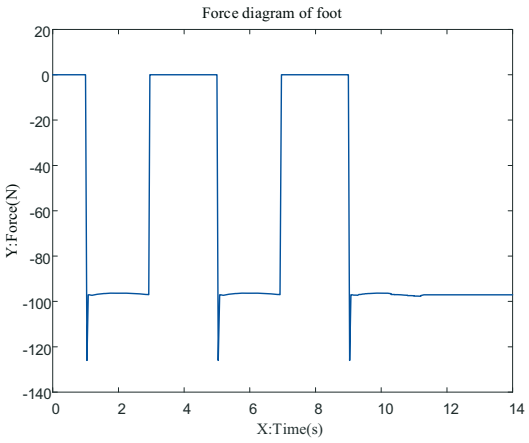

Fig. 16 Lower limb exoskeleton robot foot end force diagram

The Adams simulation shows that the foot end produces a large impact force at the moment of contact with the ground, and returns to 100 N when the curve displays a smooth state.

Figures 17 and 18 show the Simulink diagram of force level switching for classical PID control and the Simulink diagram of force level switching for fuzzy control, respectively. Force/position switching control at the foot 15 mm above the ground and according to Adams simulation results in their input position and force expectation signals respectively, then running program SimulinkCosim of simulation module for joint simulation.

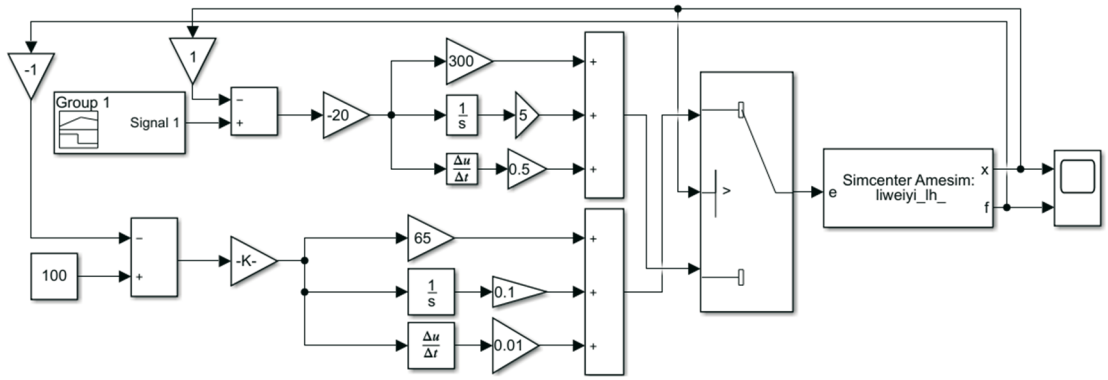

Fig. 17 Simulink diagram of force-position switching for classical PID control

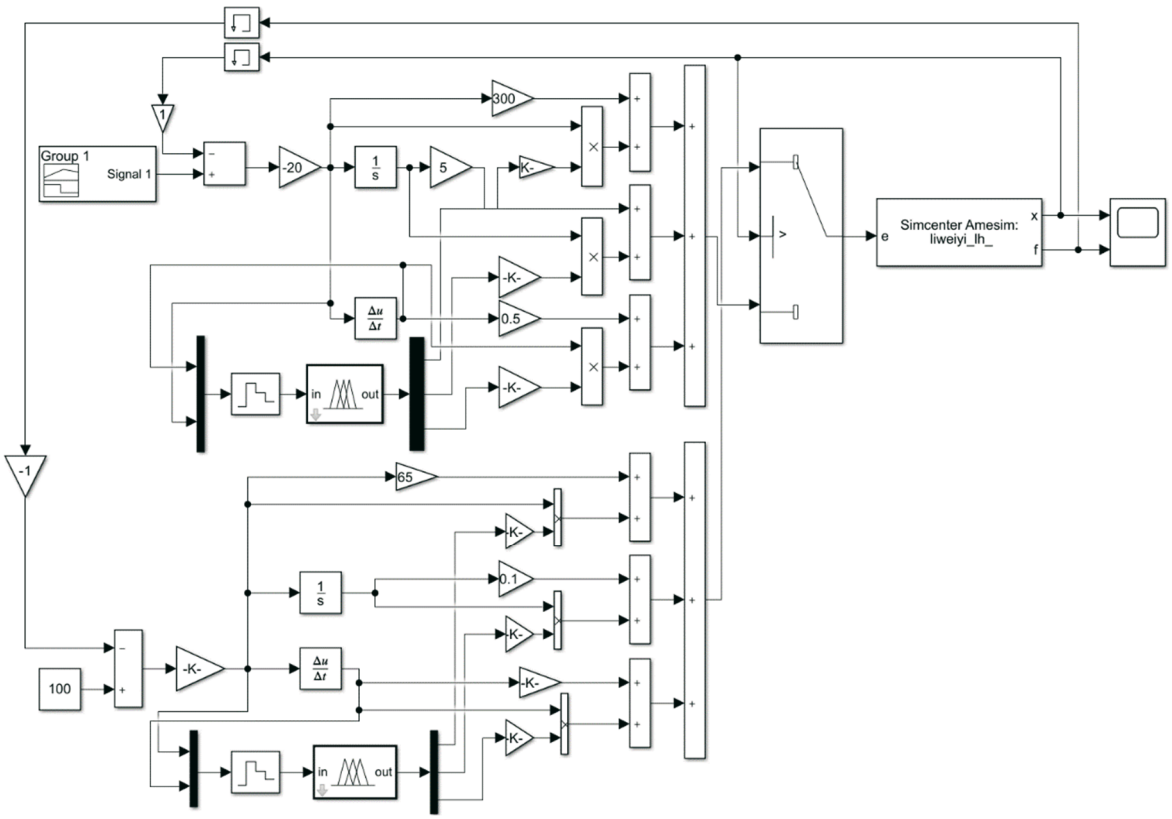

Fig. 18 Simulink diagram of fuzzy control of force level switching

4.1 Joint simulation analysis

Figure 19 shows the exoskeleton robot knee joint PID control and fuzzy control force/position switching signal diagrams, respectively. The blue curve in the Figure is the position control signal, the red curve is the actual input signal, and the black curve is the force control signal. It can be seen from the Figure that the actual input signal coincides with the position control result signal before 0.25 s, and at that time, the actual input signal is quickly switched from the position control signal to the force control signal. From the Figure, the designed switching method is able to perform force/position switching control.

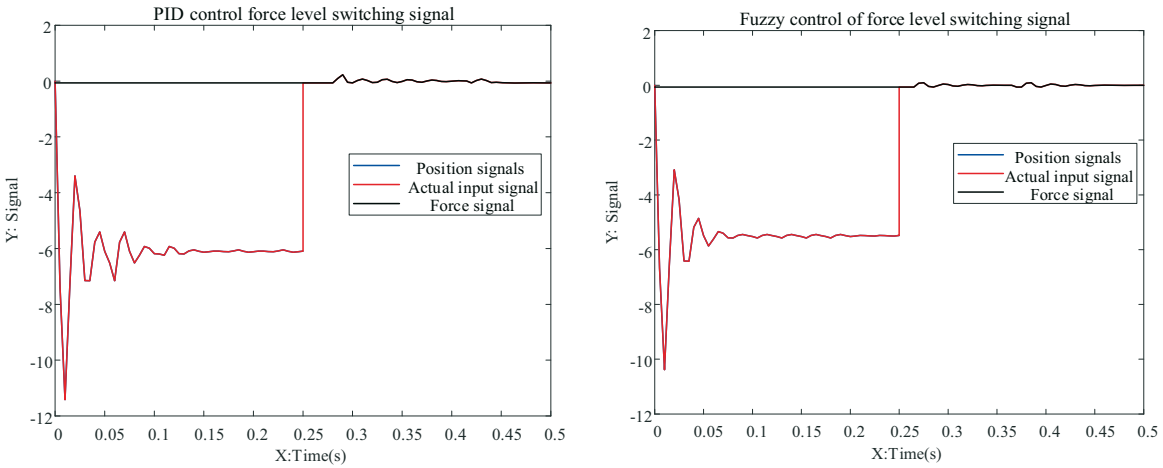

Fig. 19 Force/position switching signal diagram

Figure 20 shows the exoskeleton robot landing moment knee joint position servo system control diagram. From the simulation results in Figure 20, it can be seen that the actual displacement value under fuzzy control responds faster than the actual displacement value under PID control until 0.01 s; after 0.01 s, the change is gradually stabilised and the tracking performance is significantly better than the PID control. The analysis shows that the fuzzy control position servo system has better results than the PID control position servo system.

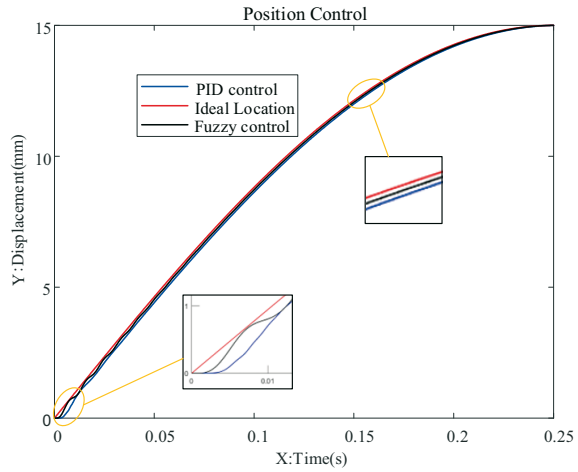

Fig. 20 Position control

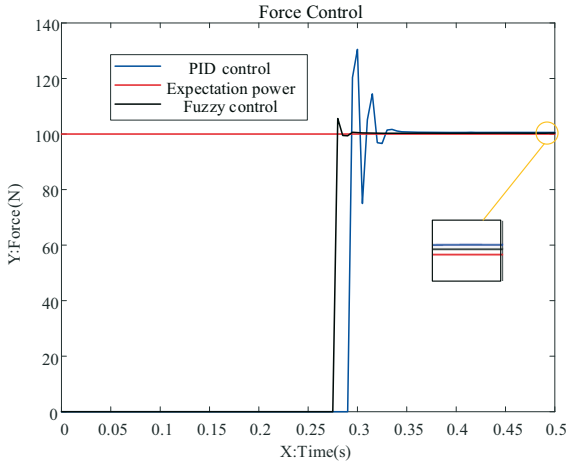

Fig. 21 Force control

Figure 21 shows the control diagram of the knee force servo system at the moment of the landing of the exoskeleton robot. The black curve in the Figure is the fuzzy control output, the blue curve is the PID control output, and the red curve is the ideal force. The graph at 0.25 s shows the faster response of fuzzy control during position switching to force, less fuzzy control jitter when the force reaches the desired value, and when the force is stable fuzzy control is closer to the ideal value than PID control. The analysis shows that fuzzy control has better flexibility in force level switching.

5. Conclusion

In order to effectively reduce the impact of the foot end of the lower limb exoskeleton robot at the moment of landing and ensure gentle contact with the ground, this paper first establishes the mathematical models for the position control system and the force control system. Then, a fuzzy control-based force/position switching active flexible control method is

proposed. The lower limb exoskeleton robot is controlled by the position servo system before it touches the ground, and switches to the force servo system at the moment it makes contact with the ground, enabling smoother landing through force/position switching. Finally, fuzzy control force/position switching is verified through a joint simulation of Amesim and Simulink and compared with PID control force/position switching. The simulation results demonstrate that the electro-hydraulic servo force/position switching method based on a fuzzy algorithm is able not only to ensure the motion accuracy of the foot end of the lower limb exoskeleton robot, but can also provide a faster response and reduced jitter during the force transition, thereby effectively improving the flexibility of the lower limb exoskeleton robot during landing.

REFERENCES

[1] LI Jianying, XIE Yinkai, XIE Shuai. Research of Control on Load System of Electro-hydraulic Load Simulator Based on Least Mean Square. China Measurement & Test, 2021,47(03):133-138.

[2] Ding Yiwei, Tu Lijuan, Liu Yixi, Progress of wearable lower limb exoskeleton rehabilitation robot, 2022, 44(5):11.

[3] LI Jianying, WANG Yunzhou, KANG Jing, SUN Xiao. Exploring Position Tracking of Electro-hydraulic Servo System with Flexible Connection CMAC Control. Mechanical Science and Technology for Aerospace Engineering, 2020,39(09): 1346-1351.

[4] Sun Han, Han Yali, Li Shenyan, et al. Design and control of hydraulically driven lower limb exoskeleton system Hydraulic and Pneumatic.2022(009):046.

[5] Kim H, Shin Y J, Kim J. Design and locomotion control of a hydraulic lower extremity exoskeleton for mobility augmentation Mechatronics, 2017, 46:32-45. https://doi.org/10.1016/j.mechatronics.2017.06.009

[6] Liu J, Xing J, Ruan X, et al. Analysis and Design of the Reconfiguration Motion Qualities of a Deformable Robot Based on a Metamorphic Mechanism. Transactions of FAMENA, 2023, 47(2): 79-97. https://doi.org/10.21278/TOF.472043022

[7] Baig R U, Dawood S, Mansour M, et al. Identifying and prioritising future robot control research with multi-criteria decision-making. Transactions of FAMENA, 2020, 44(3): 23-34. https://doi.org/10.21278/TOF.44302

[8] VMŠ Essert. Robust position control synthesis of an electro-hydraulic servo system ISA Transactions, 2010.

[9] Rybarczyk D, Milecki A. Electrohydraulic Drive with a Flow Valve Controlled by a Permanent Magnet Synchronous Motor. Transactions of FAMENA, 2020, 44(2): 31-44. https://doi.org/10.21278/TOF.44204

[10] Koivo A J, Houshangi N. Real-time vision feedback for servoing robotic manipulator with self-tuning controller IEEE Transactions on Systems Man & Cybernetics, 1991, 21(1):134-142. https://doi.org/10.1109/21.101144

[11] Fanaei A, Farrokhi M. Robust adaptive neuro-fuzzy controller for hybrid position/force control of robot manipulators in contact with unknown environment Journal of Intelligent & Fuzzy Systems, 2006, 17(2):125-144.

[12] Nichol J, Singh S, Waldron K, et al. System design of a quadrupedal galloping machine The International journal of robotics research, 2004, 23(10-11): p. 1013-1027. https://doi.org/10.1177/0278364904047391

[13] Ren Danmei. Gait planning and impedance control of a planar hydraulic bipedal robot Harbin Institute of Technology,2017.

[14] Yu B, Ba Kexian, Liu Yaliang, et al. Sensitivity analysis of control parameters of force-based impedance control method for hydraulic drive units Control and Decision, 2019(10):9.

[15] Ding Qingpeng. Stable gait theory and experimental research of quadrupedal bionic robot based on impedance control Harbin Institute of Technology,2016.

[16] Quan L, Miao Y, Guo C, et al. A Novel Composite Control Algorithm for Restraining Nonlinear Superfluous Forces. IEEE Access, 2019, 7:51841-51855. https://doi.org/10.1109/ACCESS.2019.2911400

[17] Švaco M, Vitez N, Šekoranja B, et al. Tuning of parameters for robotic contouring based on the evaluation of force deviation. Transactions of FAMENA, 2018, 42(3): 33-45. https://doi.org/10.21278/TOF.42302

[18] Wang Bingkai. Research on adaptive control of single-leg valve-controlled cylinder position of hydraulic quadruped robot Hydraulic Pneumatics and Seals,2019,39(08):29-33+40.

[19] Fan Boqian. Key technology research on hydraulically driven lower limb exoskeleton robot Zhejiang University,2017.

[20] Zhu Pingping. Research on the design of electro-hydraulic proportional position control system for nuclear environment robot based on fuzzy PID South China University, 2020.

[21] Yu, Changshun, Yuan, Rui-bo. Adaptive fuzzy PID control of electro-hydraulic position servo system based on AMESim-Simulink Agricultural Equipment and Vehicle Engineering,2022,60(08):158-161.

[22] Wang Lixin, Zhao Dingxuan, Liu Fucai et al. Self-anti-disturbance control of electro-hydraulic proportional servo force loading Journal of Mechanical Engineering,2020,56(18):216-225.

[23] Wen, Sukhwan. Study of uncertain machine human/position intelligent control and trajectory tracking experiment Yanshan University, 2005.

[24] Jin B Q, Wang Y K, Tian F. The Research for Electro-Hydraulic Servo Control System Based on Fuzzy PIDAdvanced Materials Research, 2011, 337:209-213. https://doi.org/10.4028/www.scientific.net/AMR.337.209

[25] Zaare S, Soltanpour M R. Optimal robust adaptive fuzzy backstepping control of electro-hydraulic servo position system: Transactions of the Institute of Measurement and Control, 2022, 44(6):1247-1262. https://doi.org/10.1177/01423312211051496

[26] Yu, Changshun, Yuan, Rui-bo. Adaptive fuzzy PID control of electro-hydraulic position servo system based on AMESim-Simulink Agricultural Equipment and Vehicle Engineering, 2022(008):060.

[27] Jiang, L.L., Zhang, J.J. A study on the interface and application of AMESim and Matlab/Simulink based joint simulation technology Machine Tools and Hydraulics, 2008.

Submitted: 20.5.2023

Accepted: 18.8.2023

LI Jian-ying*
School of Mechanical and Power Engineering, Harbin University of Science and Technology, Harbin 150080, China
Key Laboratory of Advanced Manufacturing and Intelligent Technology, Ministry of Education, Harbin 150080, China
WEI Ao-kun
YANG Ming-yu
WANG Ya-qian
School of Mechanical and Power Engineering, Harbin University of Science and Technology, Harbin 150080, China
*Corresponding author:
lijianying@hrbust.edu.cn